Advanced Composite Materials
Publication details, including instructions for authors and subscription information:
http://www.tandfonline.com/loi/tacm20

Vibration characteristics of composite sandwich plates and layup optimization of their laminated FRP composite faces

Hideki Sekine , Hiroshi Shirahata & Mariko Matsuda
Version of record first published: 02 Apr 2012.

To cite this article: Hideki Sekine , Hiroshi Shirahata & Mariko Matsuda (2005): Vibration characteristics of composite sandwich plates and layup optimization of their laminated FRP composite faces, Advanced Composite Materials, 14:2, 181-197

To link to this article: http://dx.doi.org/10.1163/1568551053970627

Adv. Composite Mater., Vol. 14, No. 2, pp. 181–197 (2005)

Also available online - www.vsppub.com

Vibration characteristics of composite sandwich plates and layup optimization of their laminated FRP composite faces

HIDEKI SEKINE [1,*], HIROSHI SHIRAHATA [1] and MARIKO MATSUDA [2]

[1] *Department of Aeronautics and Space Engineering, Tohoku University, Aoba-yama 01, Aoba-ku, Sendai 980-8579, Japan*
[2] *Graduate School of Engineering, Tohoku University: currently at Mechanical Engineering Research Laboratory, Kobe Steel, Ltd., Kobe, Japan*

Received 10 September 2004; accepted 9 November 2004

Abstract—This paper examines the vibration characteristics of rectangular, symmetric composite sandwich plates and the layup optimization of their top and bottom laminated FRP composite faces. The honeycomb core is modeled as a thick plate whose transverse shear deformation is taken into consideraion based on a higher-order shear deformation theory, and the top and bottom laminated FRP composite faces are modeled as a very thin sheet. A two-dimensional finite element method is developed using an eight-node isoparametric element. First, the fundamental frequency of the composite sandwich plate is discussed in the subspace of four in-plane lamination parameters of the laminated FRP composite face. Next, the layup optimization of the laminated FRP composite face for maximizing the fundamental frequency of the composite sandwich plate is performed by a nonlinear mathematical programming method, and the optimum laminate configuration of the laminated FRP composite face is determined.

Keywords: Composite sandwich plate; thin laminated FRP composite face; fundamental frequency; layup optimization; two-dimesional finite element method; higher-order shear deformation theory.

1. INTRODUCTION

A composite sandwich plate is a high-strength composite laminate which consists of a comparatively thick, light core and top and bottom thin faces, and has been widely applied to aerospace structures. Generally, the core is of honeycomb or polymer material, and the top and bottom faces are of a laminated FRP composite. To achieve performance of load-carrying capacity and stiffness of the composite sandwich plate, the design of laminate configuration of the top and bottom laminated FRP composite faces is necessary.

*To whom correspondence should be addressed.

Analytical studies of vibration problems have been conducted previously on a sandwich plate with homgeneous and isotropic faces [1, 2]. Moreover, Khatua and Cheung [3] carried out a vibration analysis of the sandwich plate with orthotropic faces using the finite element method based on a multilayer plate theory, and Ng and Das [4] using the Galerkin method for a skew sandwich plate. Mirza and Li [5] recently proposed an analytical method based on the reciprocity theorem for a vibration problem of sandwich plate.

Some researches of vibration problems [6–10] were conducted by applying the classical lamination theory and the Mindlin plate theory to the laminated FRP composite face. A vibration analysis based on a higher-order shear deformation theory was also conducted to obtain a more accurate solution [11, 12].

Few vibrational optimization problems have been studied on the composite sandwich plate. Duffy and Adali [13] examined the layup optimization using the fiber orientation angles of laminated FRP composite face as design variables, but only the angle-ply laminate configuration was studied. Therefore, sufficient design knowledge for configuring the laminated FRP composite face has not been obtained.

This study examines the vibration characteristics of rectangular, symmetric composite sandwich plates and the layup optimization of the top and bottom laminated FRP composite faces. The core is of honeycomb, and the transverse shear deformation is taken into account by applying a higher-order shear deformation theory. The top and bottom laminated FRP composite faces are sufficiently thin, compared with the core, and the in-plane and out-of-plane displacements of the top and bottom faces are uniform through the thickness. A two-dimensional finite element method is developed for the analysis using an eight-node isoparametric element. First, the fundamental frequency of the composite sandwich plate is discussed in the subspace of four in-plane lamination parameters of the laminated FRP composite face. Next, the optimization problem is formulated by using the in-plane lamination parameters as design variables. The optimum laminate configuration of the laminated FRP comosite face, which maximizes the fundamental frequency of the composite sandwich plate, is determined.

2. FREE VIBRATION ANALYSIS OF COMPOSITE SANDWICH PLATES

A rectangular, symmetric composite sandwich plate, whose core is of honeycomb, and top and bottom faces are of a laminated FRP composite, is illustrated in Fig. 1. A Cartesian coordinate system (x, y, z) is adopted, whose x and y axes run on the mid-line of two sides of the rectangular composite sandwich plate. The side lengths of the rectangular composite sandwich plate are a and b in the x and y directions, respectively, and the thickness is h. The thickness of the core is h^c, and that of the top and bottom laminated FRP composite faces is h^f. The fiber orientation angle of the laminated FRP composite face is indicated by $\theta(z)$. The deformation of the composite sandwich plate is schematically presented in Fig. 2.

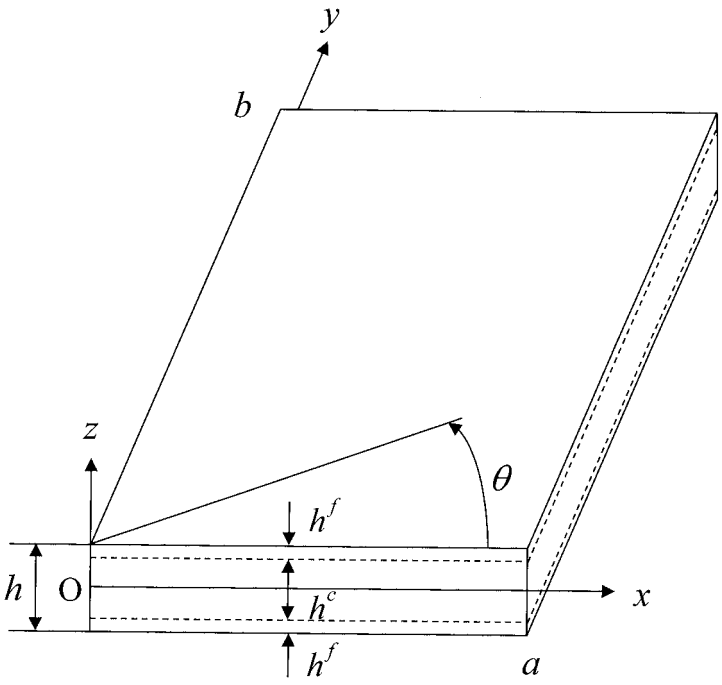

Figure 1. Rectangular, symmetric composite sandwich plate and Cartesian coordinate system.

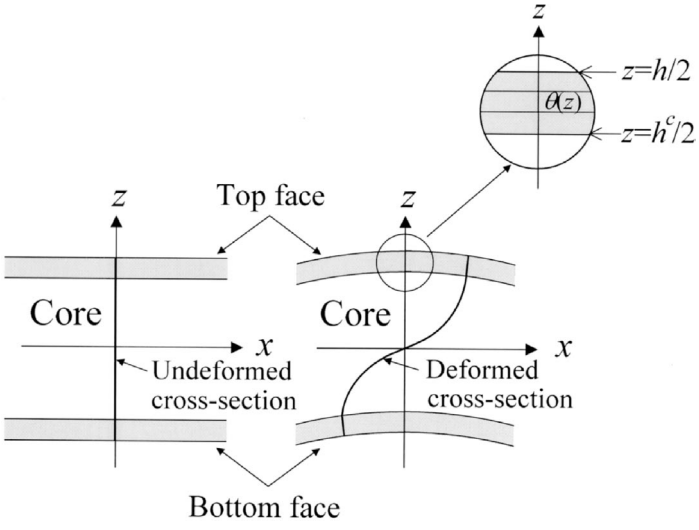

Figure 2. Schematic view of deformation of composite sandwich plate.

2.1. Elastic fields of core, and top and bottom faces

2.1.1. Core. A higher-order shear deformation theory is applied to consider the transverse shear deformation of core. By adopting a cubic function of z for the

displacements in the x and y directions u^c, v^c, and a quadratic function of z for the displacement in the z direction w^c , the displacement field is given in the following equations [14].

$$u^c(x, y, z, t) = a_0(x, y, t) + a_1(x, y, t)z + a_2(x, y, t)z^2 + a_3(x, y, t)z^3, \quad (1)$$

$$v^c(x, y, z, t) = b_0(x, y, t) + b_1(x, y, t)z + b_2(x, y, t)z^2 + b_3(x, y, t)z^3, \quad (2)$$

$$w^c(x, y, z, t) = c_0(x, y, t) + c_1(x, y, t)z + c_2(x, y, t)z^2, \quad (3)$$

where $a_0, b_0,$ and c_0 are displacements on the mid-plane of core; a_1 and b_1 are rotations of the cross-sections perpendicular to the x and y directions; and $c_1, a_2, b_2, c_2, a_3,$ and b_3 are the higher-order terms. Using equations (1) to (3), the strain $\boldsymbol{\varepsilon}^c (= [\varepsilon_x^c \varepsilon_y^c \varepsilon_z^c \gamma_{yz}^c \gamma_{zx}^c \gamma_{xy}^c]^{\mathrm{T}})$ is expressed as follows:

$$\boldsymbol{\varepsilon}^c = \boldsymbol{\varepsilon}^{c(0)} + \boldsymbol{\varepsilon}^{c(1)} z + \boldsymbol{\varepsilon}^{c(2)} z^2 + \boldsymbol{\varepsilon}^{c(3)} z^3, \quad (4)$$

where

$$[\boldsymbol{\varepsilon}^{c(0)} \boldsymbol{\varepsilon}^{c(1)} \boldsymbol{\varepsilon}^{c(2)} \boldsymbol{\varepsilon}^{c(3)}]^{\mathrm{T}} = [\mathbf{C}^{c(0)} \mathbf{C}^{c(1)} \mathbf{C}^{c(2)} \mathbf{C}^{c(3)}]^{\mathrm{T}} \mathbf{q}, \quad (5)$$

$$\mathbf{C}^{c(0)} = \begin{bmatrix} \frac{\partial}{\partial x} & 0 & 0 & 0 & 0 & 0 & 0 & 0 & 0 & 0 & 0 \\ 0 & \frac{\partial}{\partial y} & 0 & 0 & 0 & 0 & 0 & 0 & 0 & 0 & 0 \\ 0 & 0 & 0 & 0 & 0 & 1 & 0 & 0 & 0 & 0 & 0 \\ 0 & 0 & \frac{\partial}{\partial y} & 0 & 1 & 0 & 0 & 0 & 0 & 0 & 0 \\ 0 & 0 & \frac{\partial}{\partial x} & 1 & 0 & 0 & 0 & 0 & 0 & 0 & 0 \\ \frac{\partial}{\partial y} & \frac{\partial}{\partial x} & 0 & 0 & 0 & 0 & 0 & 0 & 0 & 0 & 0 \end{bmatrix}, \quad (6)$$

$$\mathbf{C}^{c(1)} = \begin{bmatrix} 0 & 0 & 0 & \frac{\partial}{\partial x} & 0 & 0 & 0 & 0 & 0 & 0 & 0 \\ 0 & 0 & 0 & 0 & \frac{\partial}{\partial y} & 0 & 0 & 0 & 0 & 0 & 0 \\ 0 & 0 & 0 & 0 & 0 & 0 & 0 & 0 & 2 & 0 & 0 \\ 0 & 0 & 0 & 0 & 0 & \frac{\partial}{\partial y} & 0 & 2 & 0 & 0 & 0 \\ 0 & 0 & 0 & 0 & 0 & \frac{\partial}{\partial x} & 2 & 0 & 0 & 0 & 0 \\ 0 & 0 & 0 & \frac{\partial}{\partial y} & \frac{\partial}{\partial x} & 0 & 0 & 0 & 0 & 0 & 0 \end{bmatrix}, \quad (7)$$

$$\mathbf{C}^{c(2)} = \begin{bmatrix} 0 & 0 & 0 & 0 & 0 & 0 & \frac{\partial}{\partial x} & 0 & 0 & 0 & 0 \\ 0 & 0 & 0 & 0 & 0 & 0 & 0 & \frac{\partial}{\partial y} & 0 & 0 & 0 \\ 0 & 0 & 0 & 0 & 0 & 0 & 0 & 0 & 0 & 0 & 0 \\ 0 & 0 & 0 & 0 & 0 & 0 & 0 & 0 & \frac{\partial}{\partial y} & 0 & 3 \\ 0 & 0 & 0 & 0 & 0 & 0 & 0 & 0 & \frac{\partial}{\partial x} & 3 & 0 \\ 0 & 0 & 0 & 0 & 0 & 0 & \frac{\partial}{\partial y} & \frac{\partial}{\partial x} & 0 & 0 & 0 \end{bmatrix}, \tag{8}$$

$$\mathbf{C}^{c(3)} = \begin{bmatrix} 0 & 0 & 0 & 0 & 0 & 0 & 0 & 0 & 0 & \frac{\partial}{\partial x} & 0 \\ 0 & 0 & 0 & 0 & 0 & 0 & 0 & 0 & 0 & 0 & \frac{\partial}{\partial y} \\ 0 & 0 & 0 & 0 & 0 & 0 & 0 & 0 & 0 & 0 & 0 \\ 0 & 0 & 0 & 0 & 0 & 0 & 0 & 0 & 0 & 0 & 0 \\ 0 & 0 & 0 & 0 & 0 & 0 & 0 & 0 & 0 & 0 & 0 \\ 0 & 0 & 0 & 0 & 0 & 0 & 0 & 0 & 0 & \frac{\partial}{\partial y} & \frac{\partial}{\partial x} \end{bmatrix}, \tag{9}$$

$$\mathbf{q} = [a_0\ b_0\ c_0\ a_1\ b_1\ c_1\ a_2\ b_2\ c_2\ a_3\ b_3]^{\mathrm{T}}. \tag{10}$$

For the honeycomb core, the stress $\boldsymbol{\sigma}^c (= [\sigma_x^c \sigma_y^c \sigma_z^c \tau_{yz}^c \tau_{zx}^c \tau_{xy}^c]^{\mathrm{T}})$ and strain $\boldsymbol{\varepsilon}^c$ relation is written as

$$\boldsymbol{\sigma}^c = \begin{bmatrix} 0 & 0 & 0 & 0 & 0 & 0 \\ 0 & 0 & 0 & 0 & 0 & 0 \\ 0 & 0 & E_z & 0 & 0 & 0 \\ 0 & 0 & 0 & G_{yz} & 0 & 0 \\ 0 & 0 & 0 & 0 & G_{zx} & 0 \\ 0 & 0 & 0 & 0 & 0 & 0 \end{bmatrix} \boldsymbol{\varepsilon}^c, \tag{11}$$

where E_z is the Young's modulus of honeycomb core in the z direction, and G_{zx} and G_{yz} are the shear moduli in the x–z and y–z planes, respectively.

2.1.2. Top and bottom faces. When the top and bottom laminated FRP composite faces are sufficiently thin, the in-plane and out-of-plane displacements of the top and bottom faces are uniform through the thickness, and the displacements agree with those on the top and bottom surfaces of core. Therefore, the displacements of the

top and bottom faces are expressed as follows:

$$u_k^f = a_0 + d_{1k}a_1 + d_{2k}a_2 + d_{3k}a_3, \tag{12}$$

$$v_k^f = b_0 + d_{1k}b_1 + d_{2k}b_2 + d_{3k}b_3, \tag{13}$$

$$w_k^f = c_0 + d_{1k}c_1 + d_{2k}c_2, \tag{14}$$

where

$$d_{1k} = -(-1)^k \frac{h^c}{2}, \quad d_{2k} = \left(\frac{h^c}{2}\right)^2, \quad d_{3k} = -(-1)^k \left(\frac{h^c}{2}\right)^3. \tag{15}$$

Here, $k = 1$ and 2 correspond to the top and bottom faces, respectively. Using equations (12) to (14), the strain of the top and bottom faces $\boldsymbol{\varepsilon}_k^f (= [\varepsilon_x^f \varepsilon_y^f \gamma_{xy}^f]^{\mathrm{T}})$ becomes

$$\boldsymbol{\varepsilon}_k^f = \mathbf{C}_k^f \mathbf{q}, \tag{16}$$

where

$$\mathbf{C}_k^f = \begin{bmatrix} \frac{\partial}{\partial x} & 0 & 0 & d_{1k}\frac{\partial}{\partial x} & 0 & 0 & d_{2k}\frac{\partial}{\partial x} & 0 & 0 & d_{3k}\frac{\partial}{\partial x} & 0 \\ 0 & \frac{\partial}{\partial y} & 0 & 0 & d_{1k}\frac{\partial}{\partial x} & 0 & 0 & d_{2k}\frac{\partial}{\partial y} & 0 & 0 & d_{3k}\frac{\partial}{\partial y} \\ \frac{\partial}{\partial y} & \frac{\partial}{\partial x} & 0 & d_{1k}\frac{\partial}{\partial y} & d_{1k}\frac{\partial}{\partial x} & 0 & d_{2k}\frac{\partial}{\partial y} & d_{2k}\frac{\partial}{\partial x} & 0 & d_{3k}\frac{\partial}{\partial y} & d_{3k}\frac{\partial}{\partial x} \end{bmatrix}. \tag{17}$$

The stress $\boldsymbol{\sigma}_k^f (= [\sigma_x^f \sigma_y^f \tau_{xy}^f]^{\mathrm{T}})$ and strain $\boldsymbol{\varepsilon}_k^f$ relation for the top and bottom laminated FRP composite faces is given by

$$\boldsymbol{\sigma}_k^f = \begin{bmatrix} Q_{11} & Q_{12} & Q_{16} \\ Q_{12} & Q_{22} & Q_{26} \\ Q_{16} & Q_{26} & Q_{66} \end{bmatrix} \boldsymbol{\varepsilon}_k^f, \tag{18}$$

where Q_{ij} are the reduced stiffnesses. The in-plane resultant stress $\mathbf{N}_k^f$ $(= [N_{xk}^f N_{yk}^f N_{xyk}^f]^{\mathrm{T}})$ and strain $\boldsymbol{\varepsilon}_k^f$ relation is written as

$$\mathbf{N}_k^f = \mathbf{A}^f \boldsymbol{\varepsilon}_k^f, \tag{19}$$

where

$$\mathbf{A}^f = \begin{bmatrix} A_{11}^f & A_{12}^f & A_{16}^f \\ A_{12}^f & A_{22}^f & A_{26}^f \\ A_{16}^f & A_{26}^f & A_{66}^f \end{bmatrix}, \tag{20}$$

$$A_{ij}^f = \int_{t_1}^{t_2} Q_{ij}\, \mathrm{d}z \quad (i, j = 1, 2, 6). \tag{21}$$

The lower and upper bounds of the integral in equation (21) are $t_1 = h^c/2$ and $t_2 = h^c/2 + h^f$ for the top face, and $t_1 = -h^c/2 - h^f$ and $t_2 = -h^c/2$ for

the bottom face. It should be noted that the in-plane stiffness A_{ij}^f is identical for the top and bottom laminated FRP composite faces because the fiber orientation is geometrically symmetric with respect to the mid-plane of composite sandwich plate. When the stiffness invariants $U_i (i = 1, 2, \ldots, 5)$ and in-plane lamination parameters $\xi_i (i = 1, 2, 3, 4)$ are introduced, the in-plane stiffnesses $A_{ij}^f (i, j = 1, 2, 6)$ are expressed as follows:

$$\begin{aligned}&\left(A_{11}^f, A_{22}^f, A_{12}^f, A_{66}^f, A_{16}^f, A_{26}^f\right)\\&\quad = h_f\{(U_1, U_2, U_4, U_5, 0, 0) + (\xi_1, -\xi_1, 0, 0, \xi_3/2, \xi_3/2)U_2\\&\qquad + (\xi_2, \xi_2, -\xi_2, -\xi_2, \xi_4, -\xi_4)U_3\}.\end{aligned} \tag{22}$$

Using the fiber orientation angle θ, the in-plane lamination parameters $\xi_i (i = 1, 2, 3, 4)$ are defined in the following equations.

$$(\xi_1, \xi_2, \xi_3, \xi_4) = \int_0^1 (\cos 2\theta, \cos 4\theta, \sin 2\theta, \sin 4\theta)\, \mathrm{d}u. \tag{23}$$

The in-plane lamination parameters $\xi_i (i = 1, 2, 3, 4)$ are dependent on each other, and the feasible region is given by [15]

$$\xi_1^2 + \xi_3^2 \leqslant 1, \tag{24}$$

$$\left(\xi_2 - \xi_1^2 + \xi_3^2\right)^2 + (\xi_4 - 2\xi_1\xi_3)^2 \leqslant \left(1 - \xi_1^2 - \xi_3^2\right)^2. \tag{25}$$

The feasible region in the case of $(\xi_3, \xi_4) = (0, 0)$ is presented by

$$2\xi_1^2 - 1 \leqslant \xi_2 \leqslant 1. \tag{26}$$

When ξ_1 and ξ_2 are prescribed, the feasible region is presented by

$$2(1 + \xi_2)\xi_3^2 - 4\xi_1\xi_3\xi_4 + \xi_4^2 \leqslant \left(\xi_2 - 2\xi_1^2 + 1\right)(1 - \xi_2). \tag{27}$$

2.2. Formulation of the two-dimensional finite element method

An equation of motion for obtaining fundamental frequency and its corresponding vibration mode of the composite sandwich plate is formulated using Hamilton's principle.

When the shape function of an eight-node two-dimensional isoparametric element is $\mathbf{N}$, $\mathbf{q}$ in equation (10) is expressed using $\bar{\mathbf{q}}$ which is $\mathbf{q}$ at the node of the element p, in the following equation.

$$\mathbf{q} = \mathbf{N}\bar{\mathbf{q}}. \tag{28}$$

By use of $\bar{\mathbf{q}}$, the strain energy of the element p is given by

$$
\begin{aligned}
U_p = & \frac{1}{2}\int_{S_p} \bar{\mathbf{q}}^{\mathrm{T}}\mathbf{N}^{\mathrm{T}}\begin{bmatrix}\mathbf{C}^{c(0)}\\ \mathbf{C}^{c(2)}\end{bmatrix}^{\mathrm{T}}\begin{bmatrix}\mathbf{A}^c & \mathbf{D}^c\\ \mathbf{D}^c & \mathbf{F}^c\end{bmatrix}\begin{bmatrix}\mathbf{C}^{c(0)}\\ \mathbf{C}^{c(2)}\end{bmatrix}\mathbf{N}\bar{\mathbf{q}}\,\mathrm{d}S_p \\
& + \frac{1}{2}\int_{S_p} \bar{\mathbf{q}}^{\mathrm{T}}\mathbf{N}^{\mathrm{T}}\begin{bmatrix}\mathbf{C}^{c(1)}\\ \mathbf{C}^{c(3)}\end{bmatrix}^{\mathrm{T}}\begin{bmatrix}\mathbf{D}^c & \mathbf{F}^c\\ \mathbf{F}^c & \mathbf{H}^c\end{bmatrix}\begin{bmatrix}\mathbf{C}^{c(1)}\\ \mathbf{C}^{c(3)}\end{bmatrix}\mathbf{N}\bar{\mathbf{q}}\,\mathrm{d}S_p \\
& + \sum_{k=1}^{2}\frac{1}{2}\int_{S_p} \bar{\mathbf{q}}^{\mathrm{T}}\mathbf{N}^{\mathrm{T}}\mathbf{C}_k^{f\mathrm{T}}\mathbf{A}^f\mathbf{C}_k^f\mathbf{N}\bar{\mathbf{q}}\,\mathrm{d}S_p, \qquad (29)
\end{aligned}
$$

where S_p is the area of the element p. In equation (29), $\mathbf{A}^c$ is the in-plane stiffness, $\mathbf{D}^c$ is the out-of-plane stiffness, and $\mathbf{F}^c$ and $\mathbf{H}^c$ are the higher-order therms, as follows:

$$
\left.\begin{aligned}
& A^c_{33} = \textstyle\int_{-h^c/2}^{h^c/2} E_z dz = h^c E_z, && A^c_{44} = \textstyle\int_{-h^c/2}^{h^c/2} G_{yz} dz = h^c G_{yz} \\
& A^c_{55} = \textstyle\int_{-h^c/2}^{h^c/2} G_{zx} dz = h^c G_{zx} && \\
& D^c_{33} = \textstyle\int_{-h^c/2}^{h^c/2} E_z z^2 dz = \frac{1}{12}h^{c3} E_z, && D^c_{44} = \textstyle\int_{-h^c/2}^{h^c/2} G_{yz} z^2 dz = \frac{1}{12}h^{c3} G_{yz} \\
& D^c_{55} = \textstyle\int_{-h^c/2}^{h^c/2} G_{zx} z^2 dz = \frac{1}{12}h^{c3} G_{zx} && \\
& F^c_{33} = \textstyle\int_{-h^c/2}^{h^c/2} E_z z^4 dz = \frac{1}{80}h^{c5} E_z, && F^c_{44} = \textstyle\int_{-h^c/2}^{h^c/2} G_{yz} z^4 dz = \frac{1}{80}h^{c5} G_{yz} \\
& F^c_{55} = \textstyle\int_{-h^c/2}^{h^c/2} G_{zx} z^4 dz = \frac{1}{80}h^{c5} G_{zx} && \\
& H^c_{33} = \textstyle\int_{-h^c/2}^{h^c/2} E_z z^6 dz = \frac{1}{448}h^{c7} E_z, && H^c_{44} = \textstyle\int_{-h^c/2}^{h^c/2} G_{yz} z^6 dz = \frac{1}{448}h^{c7} G_{yz} \\
& H^c_{55} = \textstyle\int_{-h^c/2}^{h^c/2} G_{zx} z^6 dz = \frac{1}{448}h^{c7} G_{zx} && \\
& \text{Otherwise, } A^c_{ij} = D^c_{ij} = F^c_{ij} = H^c_{ij} = 0 \quad \text{for } i, j = 1, 2, \ldots, 6. &&
\end{aligned}\right\}. \qquad (30)
$$

Similarly, the kinetic energy of the element p is presented by

$$
T_p = \frac{1}{2}\rho^c \int_{S_p} \dot{\bar{\mathbf{q}}}^{\mathrm{T}}\mathbf{N}^{\mathrm{T}}\mathbf{Z}^c\dot{\bar{\mathbf{q}}}\,\mathrm{d}S_p + \sum_{k=1}^{2}\frac{1}{2}\rho_k^f \int_{S_p} \dot{\bar{\mathbf{q}}}^{\mathrm{T}}\mathbf{N}^{\mathrm{T}}\mathbf{Z}_k^f\mathbf{N}\dot{\bar{\mathbf{q}}}\,\mathrm{d}S_p, \qquad (31)
$$

where

$$\mathbf{Z}^c = \begin{bmatrix} Z_1^c & 0 & 0 & 0 & 0 & 0 & Z_2^c & 0 & 0 & 0 & 0 \\ 0 & Z_1^c & 0 & 0 & 0 & 0 & 0 & Z_2^c & 0 & 0 & 0 \\ 0 & 0 & Z_1^c & 0 & 0 & 0 & 0 & 0 & Z_2^c & 0 & 0 \\ 0 & 0 & 0 & Z_2^c & 0 & 0 & 0 & 0 & 0 & Z_3^c & 0 \\ 0 & 0 & 0 & 0 & Z_2^c & 0 & 0 & 0 & 0 & 0 & Z_3^c \\ 0 & 0 & 0 & 0 & 0 & Z_2^c & 0 & 0 & 0 & 0 & 0 \\ Z_2^c & 0 & 0 & 0 & 0 & 0 & Z_3^c & 0 & 0 & 0 & 0 \\ 0 & Z_2^c & 0 & 0 & 0 & 0 & 0 & Z_3^c & 0 & 0 & 0 \\ 0 & 0 & Z_2^c & 0 & 0 & 0 & 0 & 0 & Z_3^c & 0 & 0 \\ 0 & 0 & 0 & Z_3^c & 0 & 0 & 0 & 0 & 0 & Z_4^c & 0 \\ 0 & 0 & 0 & 0 & Z_3^c & 0 & 0 & 0 & 0 & 0 & Z_4^c \end{bmatrix}, \tag{32}$$

$$\mathbf{z}_k^f = h^f \begin{bmatrix} 1 & 0 & 0 & d_{1k} & 0 & 0 & d_{2k} & 0 & 0 & d_{3k} & 0 \\ 0 & 1 & 0 & 0 & d_{1k} & 0 & 0 & d_{2k} & 0 & 0 & d_{3k} \\ 0 & 0 & 1 & 0 & 0 & d_{1k} & 0 & 0 & d_{2k} & 0 & 0 \\ d_{1k} & 0 & 0 & d_{1k}d_{1k} & 0 & 0 & d_{1k}d_{2k} & 0 & 0 & d_{1k}d_{3k} & 0 \\ 0 & d_{1k} & 0 & 0 & d_{1k}d_{1k} & 0 & 0 & d_{1k}d_{2k} & 0 & 0 & d_{1k}d_{3k} \\ 0 & 0 & d_{1k} & 0 & 0 & d_{1k}d_{1k} & 0 & 0 & d_{1k}d_{2k} & 0 & 0 \\ d_{2k} & 0 & 0 & d_{2k}d_{1k} & 0 & 0 & d_{2k}d_{2k} & 0 & 0 & d_{2k}d_{3k} & 0 \\ 0 & d_{2k} & 0 & 0 & d_{2k}d_{1k} & 0 & 0 & d_{2k}d_{2k} & 0 & 0 & d_{2k}d_{3k} \\ 0 & 0 & d_{2k} & 0 & 0 & d_{2k}d_{1k} & 0 & 0 & d_{2k}d_{2k} & 0 & 0 \\ d_{3k} & 0 & 0 & d_{3k}d_{1k} & 0 & 0 & d_{3k}d_{2k} & 0 & 0 & d_{3k}d_{3k} & 0 \\ 0 & d_{3k} & 0 & 0 & d_{3k}d_{1k} & 0 & 0 & d_{3k}d_{2k} & 0 & 0 & d_{3k}d_{3k} \end{bmatrix}. \tag{33}$$

In equation (31), the superimposed dot indicates the differentiation with respect to time, and ρ^c and ρ_k^f $(k = 1, 2)$ are the densities of core, and top and bottom faces, respectively. In equation (32), $Z_i^c (i = 1, 2, 3, 4)$ are as follows:

$$\left(Z_1^c, Z_2^c, Z_3^c, Z_4^c\right) = \int_{-h^c/2}^{h^c/2} (1, z^2, z^4, z^6)\, \mathrm{d}z. \tag{34}$$

Consequently, the total strain energy and the total kinetic energy are presented by

$$U = \sum_p U_p, \tag{35}$$

$$T = \sum_p T_p, \tag{36}$$

Hamilton's principle gives

$$\delta H = \int_t^{t+\Delta t} \delta(T - U)\, \mathrm{d}t = 0, \tag{37}$$

where t is time. By substituting equations (35) and (36) into equation (37), the equation of motion for free vibration is formulated as follows:

$$\mathbf{M}\ddot{\tilde{\mathbf{q}}} - \mathbf{K}\tilde{\mathbf{q}} = 0, \tag{38}$$

where $\tilde{\mathbf{q}}$ is listed from $\bar{\mathbf{q}}$ for individual nodes for the whole structure including all elements, and $\mathbf{M}$ and $\mathbf{K}$ are the mass matrix and stiffness matrix, respectively. The solution of free vibration is presented in the following form

$$\tilde{\mathbf{q}} = \boldsymbol{\phi} \mathrm{e}^{i\omega t}. \tag{39}$$

Then, the equation of motion represented by the j-th fundamental frequency ω_j and the corresponding vibration mode $\boldsymbol{\phi}_j$ is given by

$$\mathbf{K}\boldsymbol{\phi}_j = \omega_j^2 \mathbf{M}\boldsymbol{\phi}_j. \tag{40}$$

2.3. Numerical examples and consideration of results

Consider the rectangular, symmetric composite sandwich plate whose core is of aluminum honeycomb, and top and bottom faces are of a laminated CFRP composite. The aluminum honeycomb of the core is made of sheet-like aluminum foil by conducting an undulate folding and bonding alternately the parts together. The shape of each cell is a hexagon. Then, the cell wall is of one or two sheets of aluminum foil, as shown in Fig. 3. From this fact, the anisotropy appears in the shear moduli of honeycomb core G_{yz} and G_{zx}. Maerial properties of the aluminum honeycomb core are displayed in Table 1. The material properties of the CFRP composite lamina are also displayed in Table 2. For every numerical example in

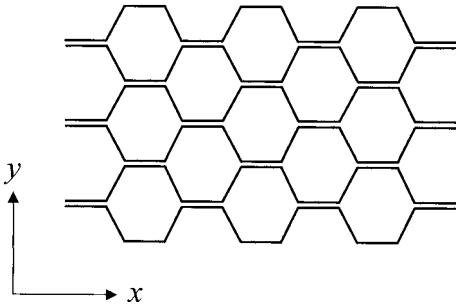

Figure 3. Schematic view of aluminum honeycomb core.

Table 1.
Material properties of aluminum honeycomb core

E_z (GPa)	G_{yz} (MPa)	G_{zx} (MPa)	ρ^c (kg/m^3)
1.09	147.1	323.6	75.0

Table 2.
Material properties of CFRP composite lamina

E_L (GPa)	E_T (GPa)	v_{LT}	G_{LT} (GPa)	ρ_k^f (kg/m^3)
153.0	10.9	0.3	5.6	1590.0

Subsection 2.3, the rectangular composite sandwich plate is simply supported on the four edges.

For the two-dimensional finite element analysis, the rectangular composite sandwich plate is divided equally into ten elements in the x and y directions, respectively. A three-dimensional finite element analysis is also conducted to verify the validity of the two-dimensional finite element analysis based on the premise that the top and bottom faces are sufficiently thin compared with the core. In the three-dimensional finite element analysis, the mesh in the x–y plane is the same as that of the two-dimensional finite element analysis, and the plate is divided into three elements corresponding to the core, and the top and bottom faces in the z direction. The element used in the three-dimensional finite element analysis is a 20-node isoparametric brick element.

Henceforth, the results of fundamental frequency are given in the following non-dimensional form

$$\omega_1^* = \omega_1 \Big/ \sqrt{\frac{E_L \times 10^{-4}}{\rho_k^f a^2}}. \tag{41}$$

2.3.1. Validating the present analysis. Figure 4 illustrates the result of non-dimensional fundamental frequency ω_1^* of the composite sandwich plate with $a/b = 1.0$ and $a/h = 20$ obtained by the present analysis and the three-dimensional finite element analysis. The top and bottom faces are of a balanced angle-ply composite

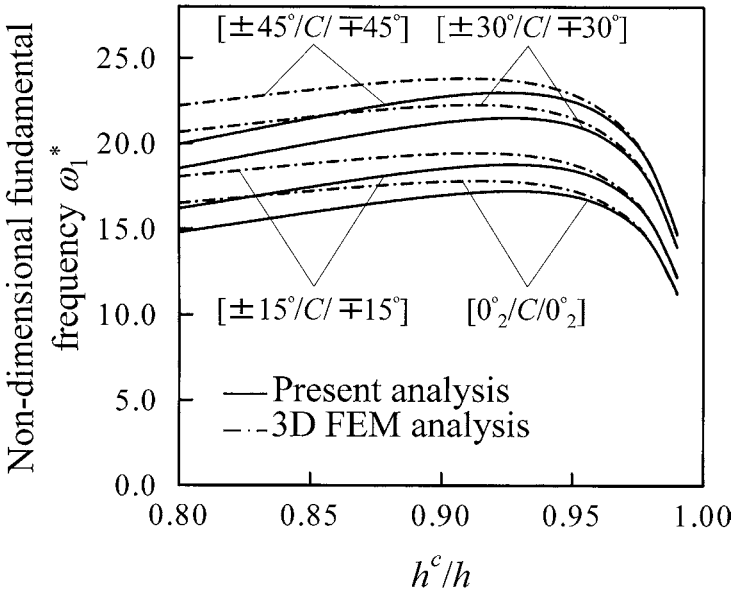

Figure 4. Comparison of the results of non-dimensional fundamental frequency ω_1^* obtained by the present analysis and the three-dimensional finite element analysis.

Table 3.
Values of non-dimensional fundamental frequency ω_1^* for $h^c/h = 0.90$ and 0.96 obtained by the present analysis and the three-dimensional finite element analysis

	$h^c/h = 0.90$			$h^c/h = 0.96$		
	Present analysis	3D FEM analysis	Error (%)	Present analysis	3D FEM analysis	Error (%)
$[0_2^\circ/\mathrm{C}/0_2^\circ]$	16.98	17.77	4.45	16.50	16.72	1.32
$[\pm 15^\circ/\mathrm{C}/\mp 15^\circ]$	18.54	19.41	4.48	17.95	18.20	1.37
$[\pm 30^\circ/\mathrm{C}/\mp 30^\circ]$	21.24	22.23	4.45	20.52	20.81	1.39
$[\pm 45^\circ/\mathrm{C}/\mp 45^\circ]$	22.76	23.79	4.33	21.84	22.12	1.27

laminate of two layers.[1] It is found from the figure that the result by the present analysis approaches that by the three-dimensional finite element analysis as the thickness ratio of the core to the composite sandwich plate h^c/h tends to one. Table 3 presents the non-dimensional fundamental frequency ω_1^* for $h^c/h = 0.90$ and 0.96 by the present analysis and the three-dimensional finite element analysis. The results differ by about 5% independent of the layup of the balanced angle-ply composite laminate for $h^c/h = 0.90$, and almost agree for $h^c/h = 0.96$. This means that the result by the present analysis is sufficiently accurate when the thickness of the top and bottom faces is sufficiently small. In this paper, the numerical calculation was therefore carried out for $h^c/h = 0.90$.

2.3.2. Vibration characteristics of rectangular composite sandwich plate. The fundamental frequency of the composite sandwich plate is discussed in the subspace of four in-plane lamination parameters of the top and bottom laminated CFRP composite faces. In Fig. 5, the contours of non-dimensional fundamental frequency ω_1^* on the plane of in-plane lamination parameter are indicated in the cases of $(\xi_3, \xi_4) = (0, 0)$, $(\xi_1, \xi_2) = (0.2, 0.5)$ and $(\xi_1, \xi_2) = (-0.2, -0.5)$ when a/b is taken as $a/b = 1.0$ and a/h as $a/h = 100, 50, 20$. It is found from the figure that ω_1^* reaches a maximum at $(\xi_3, \xi_4) = (0, 0)$ when the values of ξ_1 and ξ_2 are prescribed. This means that the existence of the in-plane extension-shear coupling, i.e., $\xi_3, \xi_4 \neq 0$, produces an effect that makes ω_1^* small. On the other hand, it is seen that ω_1^* becomes maximum on the boundary of feasible region on the $\xi_1 - \xi_2$ plane in the case of $(\xi_3, \xi_4) = (0, 0)$. It is also seen that ξ_1 at the maximum point of

[1]In the three-dimensional finite element analysis, the top and bottom two-layer laminated FRP composite faces are assumed to be of a balanced angle-ply composite laminate that the lamina with infinitesimal thickness is alternately laminated. The elastic moduli of the top and bottom faces are estimated by the rule of mixture using elastic moduli of CFRP composite lamina.

When the stacking sequence was $[\pm 30^\circ/\mathrm{C}/\mp 30^\circ]$, the non-dimensional fundamental frequency ω_1^* of the composite sandwich plate with $a/b = 1.0$, $a/h = 100$ and $h^c/h = 0.8$ was obtained as $\omega_1^* = 5.573$ by the three-dimensional finite element analysis. On the other hand, it was obtained as $\omega_1^* = 5.597$ using the Rayleigh–Ritz method. Both results agree satisfactorily.

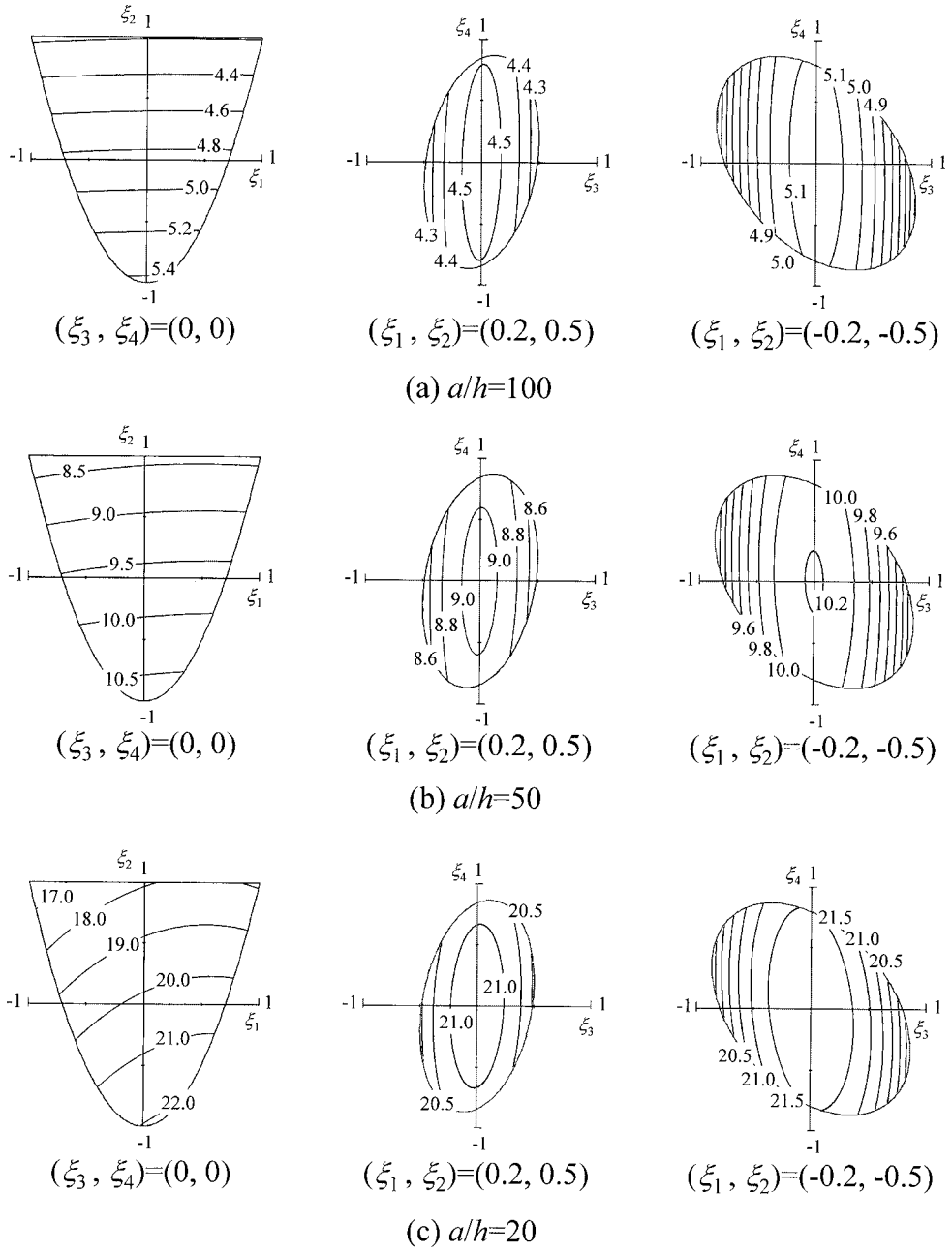

Figure 5. Contours of non-dimensional fundamental frequency ω_1^* on the plane of in-plane lamination parameter for $a/b = 1.0$ and $a/h = 100, 50, 20$.

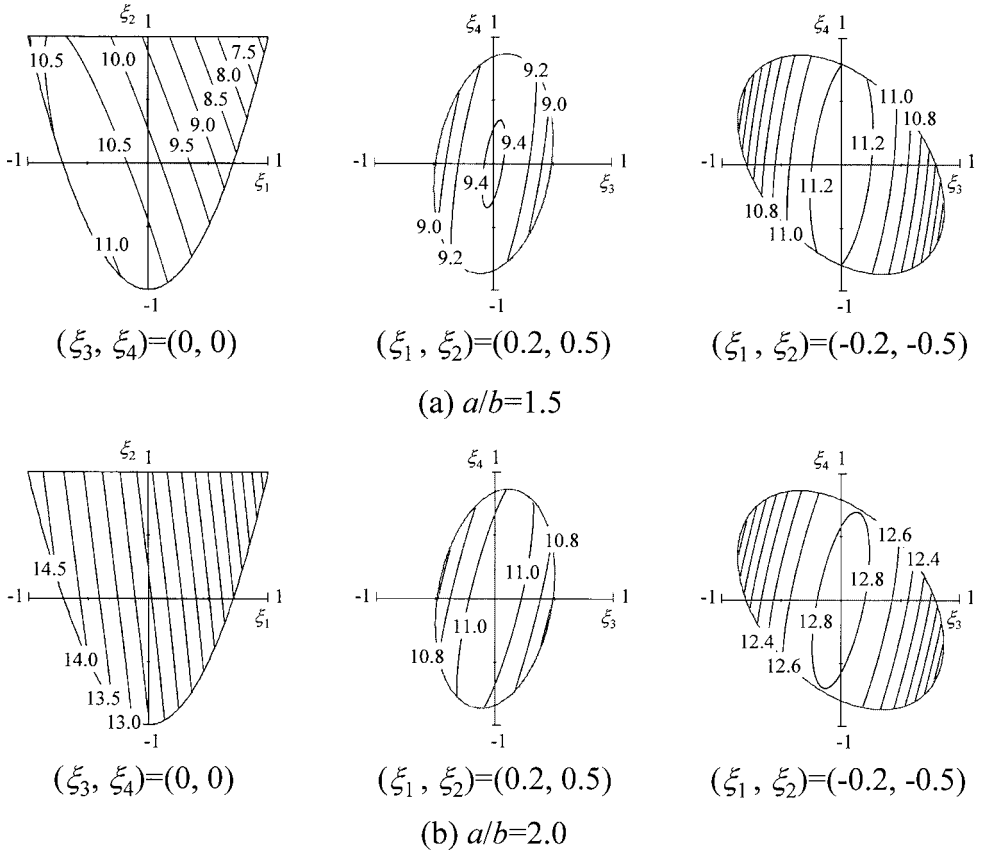

Figure 6. Contours of non-dimensional fundamental frequency ω_1^* on the plane of in-plane lamination parameter for $a/b = 1.5$, 2.0 and $a/h = 50$.

ω_1^* deviates from zero to the positive with decreasing the value of a/h. This is the effect of anisotropy of the core.[2]

Figure 6 shows the effect of the aspect ratio of the rectangular composite sandwich plate on vibration characteristics. When a/b is 1.5 and 2.0, and *a/h* is 50, the contours of non-dimensional fundamental frequency ω_1^* on the plane of in-plane lamination parameter are indicated in the cases of $(\xi_3, \xi_4) = (0, 0)$, $(\xi_1, \xi_2) = (0.2, 0.5)$ and $(\xi_1, \xi_2) = (-0.2, -0.5)$, as well as in Fig. 5. It is seen from the figure that ω_1^* becomes maximum at $(\xi_3, \xi_4) = (0, 0)$ when the values of ξ_1 and ξ_2 are prescribed. It is also observed that ω_1^* becomes maximum on the boundary of feasible region on the $\xi_1 - \xi_2$ plane in the case of $(\xi_3, \xi_4) = (0, 0)$.

[2]We numerically confirmed that ω_1^* reaches a maximum at $(\xi_1, \xi_2) = (0, -1)$ independent of the value of a/h when the core is isotropic.

3. LAYUP OPTIMIZATION OF LAMINATED FRP COMPOSITE FACES

In this section, we examine the layup optimization problem of the top and bottom laminated FRP composite faces, which maximizes the fundamental frequency of the composite sandwich plate by a nonlinear mathematical programming method. The laminate configuration of the laminated FRP composite faces is optimized using the four in-plane lamination parameters as design variables.

3.1. Formulation of the layup optimization problem

The layup optimization problem, which maximizes the fundamental frequency of the composite sandwich plate, can be formulated as

$$\begin{gathered}\text{maximize} \quad \omega_1^*(\xi_1, \xi_2, \xi_2, \xi_4),\\ \text{subject to} \quad \xi_1^2 + \xi_3^2 \leqslant 1,\\ (\xi_2 - \xi_1^2 + \xi_3^2)^2 + (\xi_4 - 2\xi_1\xi_3)^2 \leqslant (1 - \xi_1^2 - \xi_3^2)^2, \qquad (42)\\ \text{design variables} \quad \xi_1, \xi_2, \xi_3, \xi_4.\end{gathered}$$

Constraints of this layup optimization problem indicate the feasible region of in-plane lamination parameter; this feasible region is expressed by equations (24) and (25). The feasible direction method is used as an optimizer and the golden section method as a one-dimensional search in the ADS program [16].

3.2. Optimization results

Table 4 lists the values of the optimum lamination parameters and the optimum laminate configuration of the top and bottom laminated CFRP composite faces when a/b is taken as $a/b = 1.0$, 1.5, 2.0, and a/h as $a/h = 100$, 50, 20. The rectangular composite sandwich plate is simply supported and clamped on the four edges. It is recognized from the table that the optimum values of the in-plane lamination parameters ξ_3 and ξ_4 are determined as $\xi_3 = \xi_4 = 0.0$, disregarding the error of numerical calculation. The optimum laminate configuration is of angle-ply or 90° unidirectional for the simply supported composite sandwich plate, and of 0°/90° cross-ply or 90° unidirectional for the clamped one.

4. CONCLUSIONS

In this study, we have examined the vibration characteristics of rectangular, symmetric composite sandwich plates and the layup optimization of the top and bottom laminated FRP composite faces. It has been based on the premise that the top and bottom laminated FRP composite faces are sufficiently thin compared with the core.

A two-dimensional finite element method has been developed by applying a higher-order shear deformation theory and used for the present analysis.

Comparing the fundamental frequencies obtained by the present analysis and the three-dimensional finite element analysis has demonstrated that the present analysis has sufficient accuracy when the laminated FRP composite face is sufficiently thin. First, the fundamental frequency of the composite sandwich plate has been discussed in the subspace of four in-plane lamination parameters of the laminated FRP composite face. The result has proved that the in-plane extension-shear coupling produces the decrease of the fundamental frequency. Next, examining the optimum laminate configuration of the laminated FRP composite face, which maximizes the fundamental frequency of the composite sandwich plate, we have found that the maximum fundamental frequency is realized in the case of the nonexistence of in-plane extension-shear coupling. Then, the optimum laminate configuration is of angle-ply or 90° unidirectional for the simply supported composite sandwich plate, and of 0°/90° cross-ply or 90° unidirectional for the clamped one.

Table 4.
Optimum lamination parameters and laminate configuration

Boundary condition	Aspect ratio (a/b)	ω_1^*	Optimum lamination parameters				Optimum laminate configuration
			ξ_1	ξ_2	ξ_3	ξ_4	
(a) $a/h = 100$							
Simply	1.0	5.551	0.007	−1.000	−0.001	0.000	$[44.8^\circ_{0.50}/\text{-}44.8^\circ_{0.50}]$
supported	1.5	6.106	−0.560	−0.373	0.000	0.000	$[62.0^\circ_{0.50}/\text{-}62.0^\circ_{0.50}]$
	2.0	7.702	−1.000	1.000	−0.001	0.000	$[90.0^\circ]_{1.00}$
Clamped	1.0	9.104	0.441	1.000	−0.001	−0.001	$[0.0^\circ_{0.72}/90.0^\circ_{0.28}]$
	1.5	12.58	−1.000	1.000	−0.001	0.000	$[90.0^\circ_{1.00}]$
	2.0	16.49	−1.000	1.000	0.000	0.000	$[90.0^\circ_{1.00}]$
(b) $a/h = 50$							
Simply	1.0	10.71	0.013	−1.000	−0.004	0.014	$[44.6^\circ_{0.50}/\text{-}44.6^\circ_{0.50}]$
supported	1.5	11.81	−0.504	−0.493	−0.003	0.000	$[60.1^\circ_{0.50}/\text{-}60.1^\circ_{0.50}]$
	2.0	14.84	−1.000	1.000	−0.001	0.000	$[90.0^\circ_{1.00}]$
Clamped	1.0	16.98	0.443	1.000	0.002	0.000	$[0.0^\circ_{0.72}/90.0^\circ_{0.28}]$
	1.5	22.07	−1.000	1.000	−0.001	0.000	$[90.0^\circ_{1.00}]$
	2.0	28.95	−1.000	1.000	0.000	0.000	$[90.0^\circ_{1.00}]$
(c) $a/h = 20$							
Simply	1.0	23.12	0.128	−1.000	0.000	0.000	$[41.3^\circ_{0.50}/\text{-}41.3^\circ_{0.50}]$
supported	1.5	25.80	−0.361	−0.740	0.000	0.000	$[55.6^\circ_{0.50}/\text{-}55.6^\circ_{0.50}]$
	2.0	31.21	−0.876	0.531	0.000	0.000	$[75.6^\circ_{0.50}/\text{-}75.6^\circ_{0.50}]$
Clamped	1.0	32.16	0.430	1.000	0.000	0.000	$[0.0^\circ_{0.72}/90.0^\circ_{0.28}]$
	1.5	35.65	−0.266	1.000	0.000	0.000	$[0.0^\circ_{0.37}/90.0^\circ_{0.63}]$
	2.0	45.12	−1.000	1.000	0.000	0.000	$[90^\circ_{1.00}]$

REFERENCES

1. Y. Y. Yu, Flexural vibrations of elastic sandwich plates, *J. Aerospace Sci.* **27**, 272–282 (1960).
2. C. E. S. Ueng, Natural frequencies of vibration of an all-clamped rectangular sandwich panel, *Trans. ASME, J. Appl. Mech.* **33**, 683–684 (1966).
3. T. P. Khatua and Y. K. Cheung, Bending and vibration of multilayer sandwich beams and plates, *Int. J. Numer. Meth. Engng.* **6**, 11–24 (1973).
4. S. S. F. Ng and B. Das, Free vibration and buckling analysis of clamped skew sandwich plates by the Galerkin method, *J. Sound. Vib.* **107**, 97–106 (1986).
5. S. Mirza and N. Li, Analytical approach to free vibration of sandwich plates, *AIAA J.* **33**, 1988–1990 (1995).
6. H. H. Kanematsu, Y. Hirano and H. Iyama, Bending and vibration of CFRP-faced rectangular sandwich plates, *Compos. Struct.* **10**, 145–163 (1988).
7. M. Rais-Rohani and P. Marcellier, Buckling and vibration analysis of composite sandwich plates with elastic rotational edge restraints, *AIAA J.* **37**, 579–587 (1999).
8. K. Sekine, O. Ichinomiya and K. Maruyama, Bending and vibration analysis of composite rectangular sandwich plates (Effect of transverse shear deformation on face layers), *Trans. Jpn. Soc. Mech. Eng., Series C* **62**, 3908–3914 (1996) (in Japanese).
9. L. J. Lee and Y. J. Fan, Bending and vibration analysis of composite sandwich plates, *Comput. Struct.* **60**, 103–112 (1996).
10. A. Nabarrete, S. F. M. de Almeida and J. S. Hansen, Sandwich-plate vibration analysis: Three-layer quasi-three-dimensional finite element model, *AIAA J.* **41**, 1547–1555 (2003).
11. T. Kant and Mallikarjuna, A higher-order theory for free vibration of unsymmetrically laminated composite and sandwich plates: Finite element evaluations, *Comput. Struct.* **32**, 1125–1132 (1989).
12. T. Kant and K. Swaminathan, Analytical solutions for free vibration of laminated composite and sandwich plates based on a higher-order refined theory, *Compos. Struct.* **53**, 73–85 (2001).
13. K. J. Duffy and S. Adali, Optimal fibre orientation of antisymmetric hybrid laminates for maximum fundamental frequency and frequency separation, *J. Sound Vib.* **146**, 181–190 (1991).
14. S. Oskooei and J. S. Hansen, Higher-order finite element for sandwich plates, *AIAA J.* **38**, 525–533 (2000).
15. H. Fukunaga and H. Sekine, A laminate design for elastic properties of symmetric laminates with extension-shear or bending-twisting coupling, *J. Compos. Mater.* **28**, 708–731 (1994).
16. G. N. Vanderplaats and H. Sugimoto, A general-purpose optimization program for engineering design, *Comput. Struct.* **24**, 13–21 (1986).